The microphysical properties of wave PSCs retrieved from lidar measurements during SOLVE–THESEO 2000

Rong-Ming Hu, Kenneth S. Carslaw

School of the Environment, University of Leeds, Leeds, U.K.

Chris Hostetler, Lamont R. Poole

NASA Langley Research Center, Hampton, VA, USA.

Beiping Luo, Thomas Peter, Stefan Füglistaler

Laboratory for Atmospheric Physics, ETH, Zurich, Switzerland.

Thomas J. McGee, John F. Burris

Laboratory for Atmospheres, NASA Goddard Space Flight Center, Greenbelt, MD, USA.

Short title: OPTICAL AND MICROPHYSICAL PROPERTIES OF WAVE PSCS

Abstract. Mountain wave-induced ice clouds in the stratosphere are known to cause the formation of nitric acid-hydrate particles downwind. Understanding the microphysical properties of these solid particles is important because they may contribute to a general background of solid PSCs that is observed, but whose origin is not understood. Based on the limited set of observations of PSCs directly attributable to mountain waves, it has not been possible to determine their general microphysical properties. Here we analyze lidar observations from the SOLVE/THESEO-2000 campaign. Between December 1999 and March 2000 seven of the twelve flights of the DC-8 aircraft showed clear signs of mountain wave-induced clouds, with nitric acid hydrate clouds often extending many hundreds of kilometers downwind of mountains. Based on T-matrix calculations, we have developed a technique to estimate the microphysical properties of spherical and non-spherical particles from multi-wavelength backscatter and depolarization data from the GSFC/LaRC Aerosol lidar. The technique allows particle radius, condensed mass, and number densities of ice, nitric acid trihydrate and liquid PSCs to be estimated. Ice clouds were found to contain approximately 1 to 3 ppmv of condensed water with a number density from 1 to 10 cm^{-3}, and a narrow size distribution width with mode radii from 1 to 1.5 μm. Nitric acid hydrate particles downwind of the ice clouds were consistent with 1 to 5 ppbv condensed HNO$_3$, a number density from 0.5 to 2 cm^{-3}, and mode radius around 0.5 μm. These hydrate clouds are characterised by high aerosol backscatter and depolarization and are distinct from type 1a clouds that are observed away from mountains, which have low aerosol backscatter.

1. Introduction

Between December 1999 and March 2000 the NASA DC-8 made 12 flights in the Arctic vortex as part of the SAGE III Ozone Loss and Validation Experiment and the Third European Stratospheric Experiment on Ozone (SOLVE/THESEO-2000). Polar stratospheric clouds (PSCs) were observed by lidar on numerous occasions. Several flights were designed to probe wave-cloud PSCs that had been forecast to occur over the East Greenland and Scandinavian mountains. Several flights were also made by the European Falcon aircraft employing the OLEX lidar system. These flights provide a rich dataset with which to study the formation regions of different PSCs. The wave cloud flights were made possible by operational forecasts of stratospheric mountain waves over the whole Arctic region, as described by *Eckermann et al.* [2001]. In this paper, we use data from the Goddard Space Flight Center/Langley Research Center (GSFC/LaRC) lidar system, providing observations of aerosol backscatter ratio at three wavelengths (354, 532 and 1064 nm) and depolarization at one wavelength (532 nm).

Polar stratospheric wave clouds form in regions of strong adiabatic temperature perturbation. The most common cause of such localized cooling in the Arctic stratosphere is gravity waves produced by surface topography [*Peter et al.*, 1997; *Carslaw et al.*, 1998; *Wirth et al.*, 1999; *Eckermann and Preusse*, 1999; *Riviere et al.*, 2000; *Dörnbrack et al.*, 2001a,b], although adiabatic cooling may also occur in the vicinity of jet streams [*Wu and Waters*, 1996].

Observations of Arctic wave clouds using airborne lidar have shown that the strong adiabatic cooling and warming over mountains can lead to the formation of a wide range of different PSCs in close proximity [*Carslaw et al.*, 1998; *Wirth et al.*, 1999]. These studies also suggest that the wave clouds may have an effect on PSCs distant from the mountains. For example, PSCs containing solid particles (most likely nitric acid hydrates) have been observed to extend several hundred kilometers downwind of the Scandinavian mountains [*Carslaw et al.*, 1998; *Riviere et al.*, 2000] . *Carslaw et al.* [1999] used a simple parameterization of mountain wave cooling to show that the net effect of many such events in the Arctic would be to increase the fraction of the polar stratosphere containing nitric acid hydrate PSCs.

The formation mechanisms of nitric acid hydrate clouds are still not clear. Recent observations [*Biele et al.*, 2001] suggest that as much as 50% of PSCs contain solid hydrate particles, as revealed by extensive lidar observations from the Ny Ålesund ground-based station, which is representative of the deep polar vortex. Analysis of the 1989 DC-8 lidar observations in the Arctic [*Toon et al.*, 2000] suggests that at least 70% of the PSCs contained solid particles.

The contribution of mountain wave events to this general background of hydrate clouds needs to be considered. To establish what contribution mountain waves make to solid PSCs in the Arctic vortex it is necessary to understand both the climatological occurrence of the wave clouds [*Carslaw et al.*, 1999] as well as the microphysical properties of the clouds that form. Previous studies have provided a highly detailed analysis of the microphysical properties of several clouds over the Scandinavian mountains [*Carslaw et al.*, 1998; *Wirth et al.*, 1999; *Riviere et al.*, 2000]. These studies showed a clear transition from liquid PSC on the upwind side of the mountains to nitric acid hydrates downwind, with ice clouds in between and provided the first evidence for nitric acid hydrate formation in the clouds. The most important conclusion of these detailed studies, in the context of solid PSCs on the synoptic scale, was that the clouds downwind of the mountains contain > 0.2 hydrate particles cm^{-3}, and often much higher number densities were found. This number concentration is greater than occurs in the more widely observed type 1a clouds. (Two optical modelling studies have recently estimated the number concentration of hydrate particles in type 1a clouds. *Tsias et al.* [1999] suggest an upper limit of about 0.01 hydrate particles cm^{-3}, while *Toon et al.* [2000] estimate an upper limit of 1% of the available nuclei, or typically less than 0.1 cm^{-3}.) Here, we extend previous studies of mountain wave clouds by examining the microphysical properties of several clouds observed by the DC-8 aircraft during SOLVE/THESEO-2000 in December 1999 and January 2000.

2. Lidar measurement technique

The GSFC/LaRC aerosol lidar system measures profiles of aerosol and cloud backscatter at 355, 532 and 1064 nm and aerosol/cloud depolarization at 532 nm.

The LaRC Aerosol Lidar is a piggy-back instrument on the GSFC Airborne Raman Ozone and Temperature Lidar (AROTEL) lidar [*McGee et al.*, 1995; *and Burris*, 1996; *Burris et al.*, 1998]. The light source for the aerosol measurements is a Continuum 9050 Nd:YAG laser operating at 50 shots per second. The laser transmits approximately 600 mJ at 1064 nm, 250 mJ at 532 nm, and 350 mJ at 355 nm. AROTEL also employs an excimer laser transmitting at 308 nm and uses the molecular and Raman backscatter from the 355 and 308 beams to measure ozone and temperature. Backscattered light at all wavelengths is collected by a 16-inch diameter Newtonian telescope with a selectable field stop.

The signals measured by the instrument are composed of backscatter from both air molecules and aerosol/cloud particles. The aerosol/cloud component of the signal is estimated using density profiles derived from Data Assimilation Office (DAO) assimilation model results.

The archived products are produced over an altitude range extending from approximately 5 km to 20 km above the aircraft. Data are acquired at nominal resolutions of 15 m vertical and 500 m horizontal (2 s integration).

In terms of the backscatter coefficient, the total backscatter ratio and the aerosol depolarization are defined as

$$S \ = \ \frac{\beta_{\mathrm{aerosol}}}{\beta_{\mathrm{air}}} \tag{1}$$

$$\delta \ = \ \frac{\beta_{\mathrm{aerosol},\perp}}{\beta_{\mathrm{aerosol},\|}} \tag{2}$$

where β_{aerosol} is the backscatter coefficient of aerosol particles and its components $\beta_{\mathrm{aerosol},\perp}$ and $\beta_{\mathrm{aerosol},\|}$ are for perpendicular and parallel polarized radiation. β_{air} is the backscatter coefficient of the air molecules.

3. Retrieval technique

Multi-wavelength lidar measurements provide an approximate measure of particle size through the wavelength dependence of the backscatter ratio. In addition, the depolarization of a plane polarized

lidar beam can be used as a sensitive indicator of the presence of non-spherical (solid) particles.[e.g., *Poole and McCormick*, 1988; *Browell et al.*, 1990; *Toon et al.*, 1990; *McCormick et al.*, 1990; *David et al.*, 1998; *Gobbi et al.*, 1998; *Carslaw et al.*, 1998; *Tsias et al.*, 1999; *Toon et al.*, 2000].

Most investigations of PSCs using lidar focus on understanding the occurrence of different PSC 'types'; that is, whether the clouds are composed of non-depolarizing particles (indicative of liquid aerosols), depolarizing particles with moderate backscatter ratio (indicative of nitric acid hydrate particles), or depolarizing particles with high backscatter (indicative of ice particles). The aim of these studies is often to understand what controls the phase of the particles.

Recently, a few studies have attempted to quantify the microphysical properties of clouds based on lidar observations. We have previously used aircraft lidar observations of mountain wave-induced clouds together with microphysical and optical models to derive particle sizes along air parcel trajectories through the waves [*Carslaw et al.*, 1998; *Wirth et al.*, 1999]. In those studies, good agreement between the multi-wavelength lidar observations and the modeled optical properties of liquid, nitric acid hydrate, and ice clouds was obtained, allowing particle size distributions to be determined from the microphysical model. The technique of combined microphysical/optical modeling of wave clouds was particularly successful because the microphysical model provided a tight physical constraint on the size distribution of the particles at any point in the cloud. *Tsias et al.* [1999] used a similar technique to constrain the microphysical properties of a nitric acid hydrate cloud observed over the North Atlantic. Again, a microphysical model was used to constrain what microphysical properties a cloud could have, based on various assumptions.

A free retrieval of cloud microphysical properties is more difficult. A free retrieval means attempting to derive the microphysical properties of a cloud based on lidar data without the additional constraint of a microphysical model. *Toon et al.* [2000] used the calculated scattering properties of spherical and non-spherical PSC particles to infer likely sizes and number concentrations of the particles in clouds observed from the DC-8 in 1989 [*Browell et al.*, 1990]. More recently, *Luo et al.* [2001] used a look-up table of scattering properties to derive typical microphysical properties of clouds observed during the

SOLVE campaign. They were able to identify several quasi-distinct PSC types and estimate the sizes and number densities of the particles. *Li and Mishchenko* [2001] have also used the T-matrix technique to determine possible particle sizes in PSCs in a similar way, and also examined the effect of assuming cylindrical particles.

Here, we attempt to derive the microphysical properties of the clouds from the lidar observations alone. To retrieve aerosol properties from multi-wavelength scattered light intensities is a notoriously under-determined problem [*Twomey*, 1977a,b]. The ill-posedness and the associated solution ambiguity have hampered the inversion problem. Many kinds of inversion methods have been developed to try to overcome these difficulties, such as the constrained linear inversion method [*King*, 1982], statistical methods [*Rodgers*, 1976; 1990], relaxation methods [*Chahine*, 1972] or the neural networks approach [*Ishimaru et al.*, 1990]. Moreover, the positive smoothing constraint regularization combined with the least square fitting procedure has been developed for improving the constrained linear inversion method [*Liu et al.*, 1999; *Amato et al.*, 1996].

Aside from these inversion methods, the look-up table (LUT) approach, which we use here, is an attractive alternative [*Tanre et al.*, 1996, *Higurashi and Nakajima*, 1999; *Luo et al.*, 2001; *Li and Mishchenko*, 2001]. In the LUT method, a precalculated dataset of many values of aerosol scattering properties (such as backscatter ratio, depolarization, etc.) are compared with measurements until the best fit is obtained. The scattering properties in the LUT must be calculated for all desired parameters of the aerosol population that are to be retrieved.

3.1. Method

The T-Matrix light scattering algorithm [*Mishchenko*, 1993] has been used for calculating scattering by non-spherical stratospheric particles, with some success [*Carslaw et al.*, 1998; *Wirth et al.*, 1999; *Luo et al.*, 2001; *Li and Mishchenko*, 2001]. In this technique, the particles are assumed to have shapes that allow an exact calculation of scattering efficiency. In the context of analyzing lidar measurements, spheroidal, cylindrical, and Chebyshev particles have been assumed [e.g., *Mishchenko and Sassen*, 1998;

Carslaw et al., 1998; *Li and Mishchenko*, 2001].

Here, we assume the PSC particles to be spheroidal. Oblate-like particles are described by an aspect ratio $\varepsilon > 1$ and prolate particles by $\varepsilon < 1$. The good agreement between the observed and modeled PSC optical properties in our previous studies gives us confidence that the representation of non-spherical particles as spheroidal scatterers (and the use of T-matrix codes to calculate the backscattering ratio) is realistic. Here, we use look-up tables for the particle backscatter ratio at 354, 532, and 1064 nm and the aerosol depolarization at 532 nm for radii between 0.01 and 5 μm ($\Delta r = 0.05$ μm) and spheroidal aspect ratios between 0.5 and 1.5 ($\Delta\epsilon = 0.05$) [*Trautmann et al.*, 2001; *Luo et al.*, 2001].

The aerosol and cloud particle populations are assumed to be composed of lognormal modes, described by

$$\frac{dN(r)}{dr} = \frac{N}{\sqrt{2\pi}r\ln\sigma}\exp\left(-\frac{\ln^2(r/r_m)}{2\ln^2\sigma}\right), \tag{3}$$

for which the parameters to be retrieved from the lidar data are the particle number concentration (N), the (spherical-equivalent) mode radius (r_m), and the width of the lognormal mode (σ), with the refractive index defined for different types of PSC. The aspect ratio (shape) of the spheroidal particle (ε) must either be defined or taken as a further unknown. Here, we assume it to be a fourth unknown to be determined from the retrieval. The mass concentration m (particle mass per mass of air) depends on N, r_m, and σ according to

$$m = \frac{4}{3}\pi\rho r_m^3 N e^{\frac{9}{2}\ln^2\sigma}, \tag{4}$$

where ρ is the mass density of the particle.

There are therefore 4 unknown parameters of the aerosol distribution to be derived for each particle type (N, r_m, σ, and ϵ) and 4 scattering properties on which to base the retrieval (we use here 354, 532 and 1064 nm total backscatter ratio and 532 nm depolarization). The PSC type (nitric acid hydrate, liquid, or ice) is also, strictly speaking, an unknown. However, solid nitric acid hydrate clouds and liquid clouds are readily distinguished simply in terms of the aerosol depolarization (essentially zero for liquids), while ice and hydrate particles are distinguishable due to the normally very high backscatter

resulting from the much greater condensed mass of ice.

PSCs almost always contain several particle types within the same cloud element (pixel of a lidar image). For example, liquid $HNO_3/H_2SO_4/H_2O$ droplets may be present along with nitric acid hydrate particles, and both will contribute to the aerosol backscatter. Clearly, it is not possible to retrieve the full complexity of such mixed aerosol populations with just 4 scattering parameters. However, as we show in section 3.2 the retrieved microphysical properties are reasonably robust for the particular types of cloud that are found in mountain waves. Liquid (non depolarizing) clouds are likely to be well retrieved since it can be assumed that they are composed of a single particle type, although it is necessary to assume that the droplet size distribution is mono-modal. Ice clouds are also likely to be well retrieved since the scattering efficiency of the ice particles will dominate that of any interstitial hydrate or liquid particles. The problem arises with mixed hydrate/liquid clouds in which the total scattering efficiency of the droplets and crystals may be comparable. We discuss the problem of externally mixed particle populations in section 3.2.

The following steps were used to convert lidar images of scattering properties into equivalent images of microphysical properties.

Step 1: Firstly, we spatially averaged the lidar data to a resolution of 300 m vertical $\times$ 3 minutes horizontal (approximately 40 km) in order to produce a manageable number of pixels for the retrieval. For the 532 nm and 1064 nm channels, approximately 12 pixels of the original data were averaged to produce a single pixel, amounting to about 3000 averaged pixels in each of the images shown here. For the 354 nm channel, which has a lower resolution, the averaging is over 6 original pixels.

The mean value and variance of backscatter ratio and depolarization for n pixels are

$$\overline{S_\lambda} \;=\; \frac{\sum_{i=1}^{n} S_\lambda}{n} \tag{5}$$

$$\sigma_\lambda^S \;=\; \sqrt{\frac{\sum_{i=1}^{n}(S_\lambda - \overline{S_\lambda})^2}{n-1}}, \tag{6}$$

$$\overline{\delta} \;=\; \frac{\sum_{i=1}^{n} \delta}{n} \tag{7}$$

$$\sigma^{\delta} \;=\; \sqrt{\frac{\sum_{i=1}^{n}(\delta - \overline{\delta})^2}{n-1}} \tag{8}$$

where $\overline{S_\lambda}$ and σ_λ^S are the mean value and variance of backscatter ratio at a wavelength λ; $\overline{\delta}$ and σ^δ are the mean value and variance of the aerosol depolarization.

Step 2: The second step is to distinguish the three different PSC types (liquid, nitric acid hydrate, and ice) according to their optical properties. This identification is necessary since different refractive indices are used for the different particle types in the retrieval. Table 1 shows the criteria that were used to distinguish these PSC types as well as the refractive indices used in the retrieval.

Liquid and ice clouds were retrieved as single size modes. Nitric acid hydrate clouds were assumed to be composed of nitric acid trihydrate (NAT) and to be externally mixed with liquid aerosols having 10 particles cm^{-3} and a mode radius of 0.1 μm. As we show in section 3.2 the retrieved properties of the NAT particles in externally mixed liquid/NAT clouds are relatively insensitive to the assumed properties of the liquid aerosol.

Step 3: The lookup tables of S_{354}, S_{532}, S_{1064} and δ_{532} were searched using all possible combinations of particle number concentration (N), condensed mass (m), width of lognormal distribution (σ) and spheroidal aspect ratio (ϵ). Combinations of these four particle properties were identified such that the calculated optical properties were within the limits

$$\overline{S_\lambda} - \sigma_\lambda^S < S_\lambda^{\mathrm{model}} < \overline{S_\lambda} + \sigma_\lambda^S \tag{9}$$

$$\overline{\delta} - \sigma^\delta < \delta^{\mathrm{model}} < \overline{\delta} + \sigma^\delta \tag{10}$$

where $S_\lambda^{\mathrm{model}}$ and δ^{model} are the values in the look-up table. Physically reasonable upper and lower limits were put on N, m, σ and ϵ as follows:

$$
\begin{aligned}
0.01 &< \quad N \quad /\text{cm}^{-3} < 20 \\
0.01 &< \quad m \quad /\text{ppbv HNO}_3 < 15 \\
0.1 &< \quad m \quad /\text{ppmv H}_2\text{O} < 10 \\
1.05 &< \quad \sigma \quad < 1.8 \\
0.5 &< \quad \epsilon \quad < 1.5
\end{aligned} \tag{11}
$$

The particle mode radius was then determined from N, m, and σ. The range of aspect ratios used in the retrievals is defined by the range that can be calculated with the T-matrix model. Smaller and larger values cause convergence problems in the numerical solution of the equations. There are no observations that allow ϵ for stratospheric particles to be constrained.

Note that we do not attempt to accurately retrieve the properties of the clouds with very low backscatter and moderate depolarization (type 1a clouds), which we expect to have hydrate particle number densities less than 0.01 cm^{-3}. These clouds have been studied in detail by *Luo et al.* [2001]. Here, we focus on the highly backscattering solid and liquid wave clouds.

The uncertainty in the aerosol depolarization becomes large for values of depolarization less than about 0.1. In such cases, the perpendicular backscatter ratio was used in the retrieval instead.

The look-up table searching procedure results in one or more sets of N, r_m, σ and ϵ that satisfy equations 9 and 10 for each pixel. In the case of multiple solutions, we selected the most likely solution by finding the minimum of the quantity

$$
\chi^2 \; = \; \sum_\lambda \left(\frac{\overline{S_\lambda} - S_{\lambda,j}^{\text{model}}}{\sigma_\lambda^S} \right)^2 \\
+ \left(\frac{\overline{\delta} - \delta_j^{\text{model}}}{\sigma^\delta} \right)^2 \tag{12}
$$

for the j possible solutions satisfying 9 and 10. A similar method has also been used by *Martonchik et al.* [1998] in the retrieval of aerosol properties from satellite. In many cases, we found that the solutions

were clustered around a single combination of N, r_m, σ and ϵ, suggesting that a robust determination of the particle properties had been obtained. In other cases, the solution clustered around two different sets of N, r_m, σ and ϵ. In such cases, while it is possible to find the solution that is the minimum of equation 12, the retrieved particle properties are likely to be genuinely ambiguous. In the following retrieved lidar images we have not attempted to extract such highly probable alternate solutions, but plot only the solution that produced the minimum χ^2. In such cases, the existence of alternate solutions is revealed by spatially patchy retrieved microphysical properties in what might be expected to be a rather uniform cloud.

3.2. Test of the method

Several factors contribute to the uncertainty in the retrieved microphysical properties, such as the assumption that the particles are spheroids and the possible presence of more than one size mode. It is therefore important to test the retrieval method. Unfortunately there were no colocated ER-2 and DC-8 flights inside the clouds that we are examining here, so a comparison of in situ measurements and our retrieved size distributions is not possible. However, if we assume that the particles are spheroidal, we can test the reliability of the retrieval on a synthetic size distribution, which may be composed of a single particle type or be an external mixture of two types.

We have constructed a bimodal size distribution comprised of liquid aerosols with a fixed mode radius of either 0.05 or 0.15 μm and various larger modes composed either of ice or NAT. The lidar quantities S_{532}, S_{1064}, and $\delta_{532\text{nm}}$ were then computed and these values used to retrieve the particle distribution using the procedure outlined above. The uncertainty of the input scattering properties was assumed to be $\pm10\%$, which is typical of the standard deviation of grouped pixels used in the actual retrievals (see Step 1 above). For solid particles, the spheroidal aspect ratio was assumed to be 0.9 for the calculation of the lidar properties but was a free parameter in the retrieval.

Figure 1a shows the retrieval result for pure liquid aerosols with $N = 10$ cm^{-3}and $r_m = 0.05$ or 0.15 μm. The retrieved aerosol microphysical properties are in close agreement with the synthetic

input size distribution. For the synthetic size distribution with $r_m = 0.05$ μm our retrieval produces $N = 9.2$ cm^{-3} and $r_m = 0.06$ μm. With $r_m = 0.15$ μm the retrieval produces $N = 11.9$ cm^{-3} and $r_m = 0.13$ μm. The width of the synthetic lognormal size distribution used here was 1.4. The first retrieval suggests $\sigma = 1.38$ and the second $\sigma = 1.42$.

Figure 1b shows the results for a mixed liquid and NAT particle population assuming a NAT mode with three different mode radii, but in each case with the same total condensed HNO$_3$ of 1 ppbv. In this calculation, the liquid aerosol distribution was assumed to have the properties $N = 6$ cm^{-3} and $r_m = 0.11$ μm. The unknown parameters in the retrieval are the NAT number density, mode radius, width of the mode, and the spheroidal aspect ratio. Three wavelengths (354, 532, and 1064 nm) and one depolarization (532 nm) were used. The retrieved NAT particle size distributions are in rather close agreement with the input synthetic distributions. The input/output mode radii of the NAT particles are as follows: 0.5/0.45 μm, 1.5/1.46 μm, and 3.0/2.73 μm, and the input/output NAT number densities are 0.43/0.63 cm^{-3}, 0.016/0.017 cm^{-3}, and 0.002/0.003 cm^{-3}. The input asphericity was 0.9, and the retrieved value was 0.85. The retrieved condensed masses of NAT are within 15% of the input values. Much of the uncertainty in the retrieved particle properties arises from the unknown particle asphericity.

The results for ice particles are better than for NAT particles because the light scattering by the liquid aerosols becomes insignificant, and therefore the retrieval becomes less ambiguous. We assumed 1 ppmv condensed water, a number density 10 cm^{-3}, and an ice particle mode radius of 1.5 μm for the synthetic size distribution. The retrieved results were $m = 0.98$ ppmv, $N = 9.7$ cm^{-3} and $r_m = 1.45$ μm.

We have also examined the sensitivity of the retrieved NAT particle properties to varying amounts of liquid aerosol. As stated previously, the liquid aerosol is likely to be present in most air masses in which NAT particles exist, but with an unknown and probably highly variable mass. Figure 1c shows the effect of varying the amount of liquid that is assumed to be present when doing the NAT particle retrieval. Two liquid distributions were used, one with a mode radius of 0.05 μm and one with 0.15

μm. The effect on the retrieved properties of the NAT mode is small. This result suggests that realistic uncertainties in the amount of liquid aerosol that accompanies the NAT particles is unlikely to have a significant effect on the properties of the NAT particles that are retrieved.

4. Retrieved Microphysical Properties

In this section we show retrieved microphysical properties of four mountain wave-induced clouds: January 14, 2000 (a small wave cloud over E. Greenland during the transfer flight); January 25, 2000 (ice, hydrate, and liquid clouds over the Scandinavian mountains); January 23, 2000 (extensive ice and hydrate clouds over E. Greenland and N. Atlantic); December 10, 1999 (a small cloud without ice). Plate 1 shows the flight paths and the latitude and longitude versus time so that the geographical location of the various clouds can be determined from the flight time.

4.1. January 14, 2000

On January 14, 2000, the DC-8 flew a transit flight from Dryden Airbase in the United States to Kiruna, Sweden, across the Atlantic Ocean and Greenland. A distinct wave-structured PSC is apparent over the east coast of Greenland, as shown in Plate 2. A strong backscattering feature between 22 and 24 km from 7.38 to 7.41 UT, with a backscatter ratio $S > 100$ at 1064 nm and strong depolarization > 0.4 at 532 nm, is indicative of water ice particles [*Toon et al.*, 1990; *Carslaw et al.*, 1998]. The existence of the ice cloud indicates strong localized cooling at this altitude. A non-depolarizing cloud is apparent upwind of the ice, which is most likely composed of $HNO_3/H_2SO_4/H_2O$ droplets. Downwind of the ice is a tail of depolarizing particles with much lower backscatter (typically $S < 20$ at 1064 nm), which is indicative of a nitric acid hydrate cloud, as seen in close colocation with ice clouds in several other similar observations [*Carslaw et al.*, 1998; *Wirth et al.*, 1999].

Using the lidar data, we have attempted to retrieve the microphysical properties of this cloud using the backscatter ratio of three wavelengths and depolarization at one wavelength. The microphysical results are shown in Plate 3 and the different particle types referred to can be identified in Plate 3e.

The liquid aerosol cloud (7-7.3 UT) upwind of the ice cloud has a peak mass density equivalent to 3 ppbv of HNO_3 condensation into the H_2SO_4 aerosols, with a number density of approximately 10 cm^{-3}, a small mode radius of 0.15 μm and width, σ, between 1.4 and 1.8. These retrieved properties are entirely consistent with expectations for a $HNO_3/H_2SO_4/H_2O$ aerosol population.

The condensed mass of water ice in the middle of the cloud varies from 1.2 to 1.37 ppmv. The size distribution of ice particles is represented by a lognormal distribution with a total of 4-6 particles cm^{-3}, a narrow mode width, σ, of 1.3, and a mode radius of 1.5-2 μm. The shape of particles is represented by slightly non-spherical value of aspect ratio ε. The number density of ice particles is a significant fraction of the available liquid aerosols upwind, implying efficient freezing nucleation in the wave cloud, as found in earlier studies [*Carslaw et al.*, 1998; *Wirth et al.*, 1999].

The peak mass density of NAT particles is equivalent to 3 ppbv HNO_3 condensation as NAT and is rather uniform through the NAT cloud. The retrieved size and number density of the particles, in contrast, are more variable. Given that all elements of the NAT cloud are likely to have undergone very similar thermal histories, it is unlikely that this variability is real. Rather, it is likely to be a result of ambiguous retrieval. Some patches of the NAT cloud contain approximately 0.4 particles cm^{-3}, while others contain approximately 5 particles cm^{-3}. These variations are reflected also in the retrieved mode radius, which varies between about 0.2 and 0.7 μm. In all cases, a narrow width of the NAT mode, $\sigma \sim 1.1$, is indicated (not shown). Although the retrieved properties of the NAT cloud are uncertain, the results do indicate that the number density is rather high compared with typical type 1a clouds.

4.2. January 25, 2000

On January 25, 2000, the DC-8 flew from Norway to Spitzbergen, then returned near the coast of Norway, and finally flew two short legs across the Scandinavia mountains. One aim of this flight was to investigate PSC processes through mountain waves that had been forecast (see *Eckermann et al.*, 2001 for a summary of the mesoscale forecasts for this flight).

Plate 4 shows the lidar observations during the two consecutive flight legs over the Scandinavian

mountains (note the reversal of flight direction, which can be seen in Plate 1). The two optically thick ice clouds were present directly over the mountains, with the hydrate clouds occurring downwind (east of the mountains). There is a very clear association between the ice clouds and the hydrate clouds, which strongly suggests that the hydrate particles were formed heterogeneously on ice.

Our retrieval results (Plate 5) are consistent with an ice cloud containing about 2 ppmv water, with a number density of 5-10 cm^{-3} and a mode radius of approximately 1.6 μm. The hydrate PSCs are consistent with an average 3 ppbv condensed HNO_3. Again, the optical properties of the hydrate cloud are consistent with a NAT particle number densities of either 0.3 cm^{-3} or about 2 cm^{-3}. The lognormal width, σ, is about 1.2. Such a narrow width is consistent with the microphysical model simulations of NAT particles evolving downwind of a mountain wave ice cloud [*Tsias et al.*, 1999]. The liquid cloud is composed of small spherical particles with 1-3 ppbv HNO_3 condensed as $HNO_3/H_2SO_4/H_2O$ droplets with a number density from 10-15 cm^{-3} and a mode radius < 0.3 μm. The other derived microphysical properties are summarized in Table 2.

As in previous studies [*Carslaw et al.*, 1998; *Wirth et al.*, 1999] we find that the number density of hydrate particles is less than that of the ice particles. Thus, not all ice particles are effective as nucleation sites for nitric acid hydrates, the reason for which was explored by *Wirth et al.* [1999].

4.3. January 23, 2000

On January 23, the DC-8 first flew over the Scandinavian mountains to eastern Greenland, and finally back to Kiruna, Sweden. One aim of this flight was to probe the wave clouds over the Greenland mountains that had been forecast by the MWFM mesoscale forecast model [*Eckermann et al.*, 2001].

Plate 6 shows the lidar observations for a short period of the flight during which DC-8 flew eastwards from the east Greenland coast over the Atlantic Ocean. Both hydrate and liquid PSCs are apparent in this image. We do not show the optically very dense ice cloud which occurred just to the west and immediately upwind of this cloud. Again, the three principal PSC types ice, NAT and liquid were present in close proximity. There are large amplitude wave-like structures apparent in the aerosol

and cloud layers.

Our retrieval results (Plate 7) are consistent with a PSC containing NAT particles with 1-5 ppbv HNO_3, a number density from 0.5-5 particles cm^{-3}, a very narrow width of log-normal size distribution, and mode radius 0.5-1 μm. Again, the range of retrieved properties is due to solution ambiguity rather than real variations within the cloud and, as before, the retrieved quantities cluster about two main values. The liquid cloud is composed of small droplets with 1-3 ppbv HNO_3 in the $HNO_3/H_2SO_4/H_2O$ solutions, with the number density from 10-15 particles cm^{-3}, and a small mode radius less than 0.3 μm.

4.4. December 10, 1999

Each of the wave clouds described so far was associated with ice cloud formation and identifiable mountain wave-driven localized cooling. A second type of solid nitric acid wave cloud was also apparent during a flight over Spitzbergen on December 5, 1999 and over Franz Josef Land [82 °N, 60 °E] on December 10, 1999. On December 10, 1999, the DC-8 flew from Kiruna, Sweden towards eastern Greenland, passed Spitzbergen, then returned to Kiruna. A PSC was observed between 13.5 and 14.5 UT, poleward of about 82 °N, between 18 to 22 km altitude (Plate 8).

The cloud shown in Plate 8 has a backscatter ratio at 1064 nm approximately a factor 10 lower than the clouds on January 23 and 25, and a depolarization at 532 nm approximately a factor of 5 lower. The temperature on the 50 hPa surface in this area was greater than 190.5 K. There is no evidence for ice formation as in the previous clouds, although neither can an ice-mediated formation mechanism for the solid nitric acid particles be excluded from the data. The cloud has a clear wave-like structure, which may indicate a localized gravity wave-driven cooling and formation of nitric acid hydrate particles.

Our retrieval results (Plate 9) indicate that this PSC is consistent with a condensed HNO_3 amount of 0.5 ppbv, but with a rather poorly defined number density and size of the NAT particles. As was the case for the January 14 PSC, the NAT number density appears to be either around 0.03 cm^{-3} or

around 0.4 cm^{-3}, with a mode radius of either 1-1.5 μm or 0.4 μm, respectively.

5. Summary and discussion

Lidar observations during SOLVE have been used to examine the microphysical properties of PSCs formed by adiabatic cooling in mountain-induced gravity waves. Patterns of cloud occurrence are similar to those found in previous aircraft observations of mountain waves; namely, liquid PSCs upwind of the mountains, ice clouds directly over the mountains, and predominantly nitric acid hydrate clouds downwind of the mountains. The wave clouds observed during the January deployment of the DC-8 were less clear in their structure than earlier observations [*Carslaw et al.*, 1998; *Wirth et al.*, 1999], making it difficult to construct air parcel trajectories based on visible wave features. Our approach has therefore been to attempt a retrieval of cloud microphysical properties using the optical information alone.

Our technique of retrieving PSC microphysical properties from multi-wavelength lidar data (see also *Luo et al.* [2001]) has been tested and shown to be effective for the types of clouds that form in mountain waves. The wave clouds contain relatively high number densities of particles with sizes comparable to the lidar wavelength. However, as shown by *Luo et al.* [2001] the retrieval technique can only be used to define particle size limits in cases where the particles are very much larger than the lidar wavelength. Even for the wave clouds, we have shown that the retrieved microphysical properties can be quite variable throughout a cloud that appears to have rather uniform aerosol backscatter. Such solution ambiguity is apparent as the speckled regions of the clouds in Plates 3, 5, 7 and 9. We plan to undertake a similar study using additional lidar wavelengths to see if a the retrieval can be improved. Comparisons of our retrieved particle sizes with in situ particle size distribution measurements from balloons or aircraft would also be useful.

A clear picture of the types of clouds produced by mountain wave cooling is now emerging. The optical properties of the different wave-induced clouds observed during SOLVE were similar to previous observations of clouds that were attributed to mountain waves [*Carslaw et al.*, 1998; *Wirth et al.*,

1998]. Ice clouds were observed in the coldest parts of the gravity waves and contain high number densities (typically 5-10 cm^{-3}) of ice particles (see Table 2), which is consistent with rapid homogeneous nucleation of ice from liquid aerosols at low temperatures [*Koop et al.*, 2000]. The nitric acid hydrate clouds downwind of the ice, which we assume to be composed of NAT particles, have a comparatively high backscatter ratio ($S = 2$ at 532 nm) and high aerosol depolarization ($\delta = 0.1 - 0.2$ at 532 nm), which contrasts markedly with the very low backscatter ratio of the more ubiquitous type 1a hydrate clouds [*Toon et al.*, 1990; *Biele et al.*, 2001] that are not obviously associated with mountain-wave effects. The optical properties of the wave-induced hydrate clouds are consistent with a high number density (0.3-5 cm^{-3}) of small (radii < 1 μm) hydrate particles (see Table 2), compared with less than 0.01 cm^{-3} and radii > 3 μm that are likely to be present in type 1a clouds [*Tsias et al.*, 1999]. Earlier studies [*Carslaw et al.*, 1998; *Wirth et al.*, 1999] have shown that the high number densities of hydrate particles is consistent with heterogeneous nucleation on ice in the waves, although we have not been able to confirm this mechanism here.

It has been suggested that the action of many mountain waves in the Arctic polar vortex could be a significant source of NAT particles [*Carslaw et al.*, 1999]. An important question is whether these particles could contribute to a general background of large particles [*Fahey et al.*, 2001] that are responsible for denitrification. Particles with a radius of 0.5-1.0 μm (the mode radius of our retrieved distribution) have a fall velocity of approximately 0.1 mm s^{-1}, which is too low to be of importance: such particles fall less than 10 m in a day. We see no evidence for particles much larger than 0.5-1.0 μm in the wave clouds we have analyzed. The only way that mountain wave-generated hydrate clouds could produce much larger particles is if the air below the cloud were supersaturated with respect to the hydrate. If this were the case, particles could sediment and then grow at a much increased rate since the gas phase HNO$_3$ would not reduced by the presence of a high number density of hydrate particles. We explore this possibility in *Füglistaler et al.* [2002].

References

Amato, U., D. DiBello, F. Esposito, C. Serio, G. Pavese, and F. Romano, Intercomparing the Twomey method with a multimodel lognormal approach to retrieve the aerosol size distribution. *J. Geophys. Res., 101*, 19267-19275, 1996.

Biele, J., A. Tsias, K.S. Carslaw, T. Peter, R. Neuber, Coexistence of solid and liquid particles in Arctic stratospheric clouds studied by lidar in winters 94/95 to 96/97, *J. Geophys. Res., in press*, 2001.

Browell, E.V., C.F. Butler, S. Iamail, P.A. Robinette, A.F. Carter, N.S. Higdon, O.B. Toon, M.R. Schoeberl, A.F. Tuck, Airbone lidar observations in the wintertime Arctic stratosphere: Polar stratospheric clouds, *Geophys. Res. Lett., 17*, 385-388, 1990.

Burris, J., W. Heaps, B. Gary, W. Hoegy, L. Lait, T. McGee, and M. Gross, Lidar temperature measurements during the TOTE/VOTE Mission, *J. Geophys. Res., 103*, 3505-3510, 1998.

Carslaw, K.S., M. Wirth, A. Tsias, B.P. Luo, A. Dornbrack, M. Leutbecher, H. Volkert, W. Renger, J.T. Bacmeister, T. Peter, Particle microphysics and chemistry in remotely observed mountain polar stratospheric clouds, *J.Geophys.Res., 103*, 5785-5796, 1998.

Chahine, M. T., A general relaxation method for inverse solution of full radiative transfer equation, *J. Atmos. Sci., 29*, 741-747, 1972.

David, C., C., S. Bekki, S. Godin, and G. Megie, Polar stratospheric clouds climatology over Dumont d'Urville between 1989 and 1993 and the influence of volcanic aerosols on their formation. *J. Geophys. Res., 103*, 22163-22180, 1998.

Dörnbrack, A., M. Leutbecher, J. Reichardt, A. Behrendt, K.P. Muller, and G. Baumgarten, Relevance of mountain wave cooling for the formation of polar stratospheric clouds over Scandinavia: Mesoscale dynamics and observations for January 1997, *J. Geophys. Res, 106* 1569-1581, 2001a.

Dörnbrack, A., and M. Leutbecher, Relevance of mountain waves for the formation of polar stratospheric clouds over Scandinavia: A 20 year climatology, *J. Geophys. Res, 106* 1583-1593, 2001b.

Eckermann, S.D., and P. Preusse, Global measurements of stratospheric mountain waves from space, *Science, 286*, 1534-1537, 1999.

Eckermann, S.D., A. Dörnbrack, S. Vosper, and K.S. Carslaw, Mesoscale forecasting of the stratosphere during SOLVE-THESEO 2000, submitted to *J. Geophys. Res.*, 2001.

Fahey, D.W., et al., The detection of large HNO$_3$-containing particles in the winter Arctic stratosphere *Science, 291*, 1026-1031, 2001

Fu, Q., and K.N. Liou, Parameterization of the radiative properties of cirrus clouds, *J.Atmos.Sci., 50*, 2008-2025, 1993.

Gobbi, G.P., G. Di Donfrancesco, and A. Adriani, Physical properties of stratospheric clouds observed during the Antarctic late winter of 1992, *J. Geophys. Res., 103*, 10859, 1998.

Heaps, W., and J. Burris, Airborne Raman Lidar, *Appl. Opt., 35,* 7128, 1996.

Higurashi, A., and T. Nakajima, Development of a two-channel aerosol retrieval algorithm on a global scale using NOAA AVHRR, *J. Atmos. Sci.*, 924-941, 1999.

Ishimaru, A., R.J. MarksII, L. Tsang, C.M. Lam, and D.C. Park, Particle-size distribution determination using optical sensing and neural networks, *Opt. Lett., 15*, 1221-1223., 1990.

King, M. D., Sensitivity of constrained linear inversions to the selection of the Lagrange multiplier, *J. Atmos. Sci.*, 10341-10356, 1994.

Koop, T., B.P. Luo, A. Tsias, and T. Peter, Water activity as the determinant for homogeneous ice nucleation in aqueous solutions, *Nature, 406*, 611-614, 2000.

Liu, L., and M. I. Mishchenko, Constraints on PSC particle microphysics derived from lidar observations, *J. Quant. Spectrosc. Radiat. Transfer, 70*, 817-831, 2001.

Liu, Y., W.P. Arnott, and J. Hallett, Particle size distribution retrieval from multispectral optical depth: Influences of particle nonsphericity and refractive index, *J. Geophys. Res., 104*, 31,753-31762, 1999.

Luo, B.P., T. Peter, S.A. Fueglistaler, H. Wernli, R.M. Hu, K.S. Carslaw, C.A. Hostetler, L. A. Poole, T. J. McGee and J.F. Burris, Large stratospheric particles observed by lidar during the SOLVE/THESEO 2000 mission, *J. Geophys. Res, submitted*, 2001.

Martonichik, J. V., D.J. Diner, R. Kahn, T.P. Ackerman, M. M. Verstraete, B. Pinty, H. R. Gordon, Technique for retrieval of aerosol properties over land and ocean using multi-angle Image. Submitted to *IEEE transaction on Geoscience and Remote sensing*, 48pp, 1997.

McCormick, M.P., G.S. Kent, W.H. Hunt, M.T. Osborne, L.R. Poole, and M.C. Pitts, Arctic polar stratospheric cloud observations by lidar. *Geophys. Res. Lett., 17*, 381, 1990.

McGee, T., M. Gross, U. Singh, J. Butler, and P. Kimvilankani, An improved stratospheric ozone lidar, *Opt.*

Eng., *34*, 1421, 1995.

Mishchenko, M.I., Light scattering by size-shape distributions of randomly oriented axially symmetric particles of a size comparable to wavelength, *Appl. Opt., 32*, 4652-4666, 1993.

Mishchenko, M.I., K. Sassen, Depolarization of lidar returns by small ice crystals: An application to contrails, *Geophys. Res. Lett., 25*, 309-312, 1998.

Peter, T., Microphysics and heterogeneous chemistry of polar stratospheric clouds. *Ann. Rev. Phys. Chem., 48*, 779-816, 1997.

Poole, L.R., M.P. McCormick, W.H. Hunt, M.T. Osborn, S. Schaffner, and M. C. Pitts, Dual-polarization lidar observations of polar stratospheric cloud evolution. *Geophys. Res. Lett., 17*, 389, 1990.

Riviere, E.D., et al., Role of lee waves in the formation of solid polar stratospheric clouds: Case studies from February 1997, *J. Geophys. Res., 105*, 6845-6853, 2000.

Rodgers, C.D., Retrieval of atmospheric temperature and composition from remote measurements of thermal radiation, *Rev. Geophys., 14*, 609-624, 1976.

Tanre, D., D., M. Herman, Y.J. Kaufman, Information on aerosol size distribution contained in solar reflected spectral radiances, *J. Geophys. Res., 101*, 19043-19060, 1996.

Toon, O. B., E.V. Browell, S. Kine, and J. Jordan, An analysis of lidar observations of polar stratospheric clouds, *Geophys, Res. Lett., 17*, 393-396, 1990.

Toon, O.B., A. Tabazadeh, E.V. Browell, and J. Jordan, Analysis of lidar observations of Arctic polar stratosphericclouds during January 1989, *J. Geophys. Res., 105*, 20589-20615, 2000.

Trautmann, T., B.P. Luo, T. Peter, Application of T-matrix light scattering theory to polar stratospheric clouds: a database for interpreting lidar backscattering observations, *Applied Optics, submitted*, 2001.

Tsias, A., M. Wirth, K.S. Carslaw, J. Biele, H. Mehrtens, J. Reichardt, C. Wedekind, V. Weib, W.Renger, R. Neuber, U. von Zahn, B. Stein, V. Santacesaria, L. Stefanutti, F. Fierli, J. Bacmeister, and T. Peter, Aircraft lidar observation of an enhanced type Ia polar stratospheric clouds during APE-POLECAT. *J. Geophys. Res., 94*, 23,961-23969, 1999.

Twomey, S.A., The influence of pollution on the short wave albedo of clouds, *J. Atmos. Sci., 34*,1149-1152, 1977a.

Twomey, S.A., Introduction to the mathematics of inversion in remote sensing and indirect measurements, in

Developments in Geomathematics, vol.3, 243pp., Elsevier Sci., New York, 1977b.

Wirth, M., A. Tsias, A. Dornbrack, V. Weiss, K.S. Carslaw, M.Leutbecher, W. Renger, H. Volkert, T. Peter, Model-guided Lagrangian observation and simulation of mountain polar stratospheric clouds, *J. Geophys. Res*, *104*, 23971-23981, 1999.

Wu, D.L., and J.W. Waters, Gravity-wave-scale temperature fluctuations seen by the UARS Microwave Limb Sounder, *Geophys. Res. Lett., 23*, 3289-3292, 1996a.

J. F. Burris, T. J. Mcgee, Laboratory for Atmospheres, Code 916, NASA Goddard Space Flight Center, Greenbelt, MD20771, USA (e-mail: mcgee@aeolus.gsfc.nasa.gov)

K. S. Carslaw, R. M. Hu, School of the Environment, University of Leeds, Leeds LS2 9JT, U.K. (e-mail: carslaw@env.leeds.ac.uk; hu@env.leeds.ac.uk).

S. Fuglistaler, B. P. Luo, T. Peter, Laboratory for Atmospheric Physics (LAPETH), ETH, Zurich, Switzerland. (email: stefanf@atmos.umnw.ethz.ch; luo@atmos.umnw.ethz.ch; tom@atmos.umnw.ethz.ch,)

Chris Hostetler, Lamont R. Poole, NASA Langley Research Center, Mail Stop 417, Hampton, VA 23681-2199, (e-mail: c.a.hostetler@larc.nasa.gov; l.r.poole@larc.nasa.gov)

Table 1. Classification of PSC particle types, based on 1064 nm lidar backscatter ratio and 532 nm aerosol depolarization

Particle type	Backscatter ratio (S)	Aerosol depolarization (δ)	Refractive index
Background aerosol	$S < 0.1$	$\delta < 0.03$	1.42
Liquid PSC	$S > 0.1$	$\delta < 0.03$	1.42
NAT	$0.1 < S < 50$	$\delta > 0.03$	1.48
ice	$S > 50$	$\delta > 0.03$	1.32

Table 2. Summary of retrieved microphysical properties of ice and nitric acid trihydrate wave clouds

	ice			NAT		
	N	m	r_m	N	m	r_m
	(cm^{-3})	(ppm)	(μm)	(cm^{-3})	(ppb)	(μm)
December 10, 1999				0.03-0.4	0.4-1.0	0.4-1.5
January 14, 2000	4.0-6.0	$1.2 - 1.4$	1.5-2.0	0.4-5.0	2.5-4.0	0.2-0.7
January 23, 2000	5.0-10.0	$1.0 - 2.0$	1.7-2.0	0.5-5.0	1.0-5.0	0.5-1.0
January 25, 2000	5.0-10.0	$2.0 - 5.0$	1.6-2.0	0.3-2.0	1.0-3.5	0.4-1.0

Note that the stated ranges do not imply positive correlation between the different retrieved quantities.
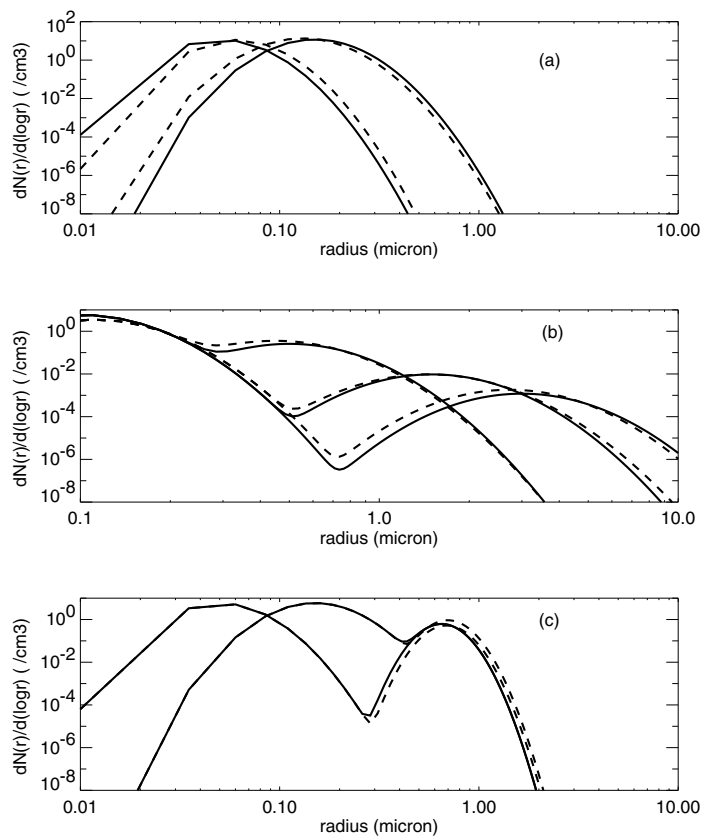
Figure 1. Retrieval of particle size distributions for synthetic particle distributions. (a) Liquid aerosols only, with mode radii of 0.05 and 0.15 μm; (b) mixed liquid/NAT particles, assuming a liquid mode radius of 0.11 μm and NAT mode radii of 0.5, 1.5 and 3.0 μm, each with a total mass of 1 ppbv condensed HNO_3; (c) the effect of varying the liquid aerosol mass assumed to be present when retrieving the properties of the solid particles. Solid line – the input synthetic size distribution; dashed line – the retrieved size distribution.
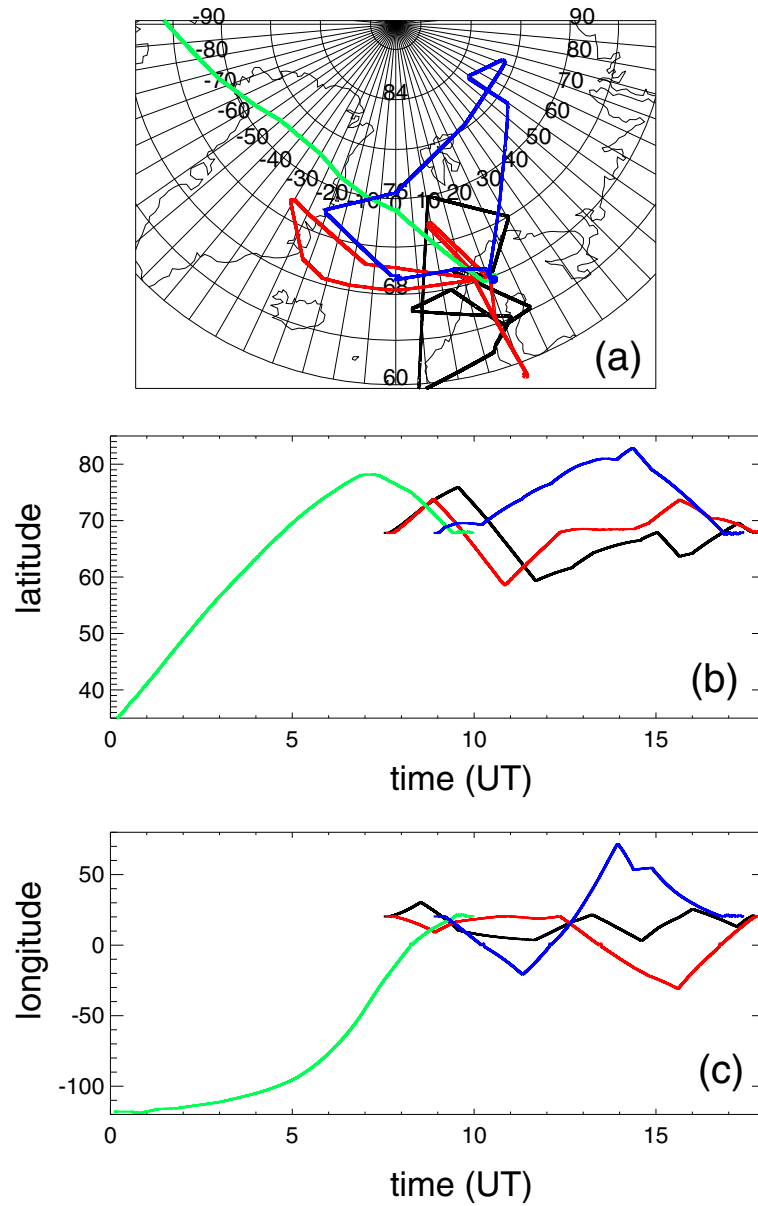
Plate 1. Flight paths of the DC-8 aircraft analysed in this paper. January 25, 2000 (black line); January 23, 2000 (red line); January 14, 2000 (green line); December 10, 1999 (blue line).
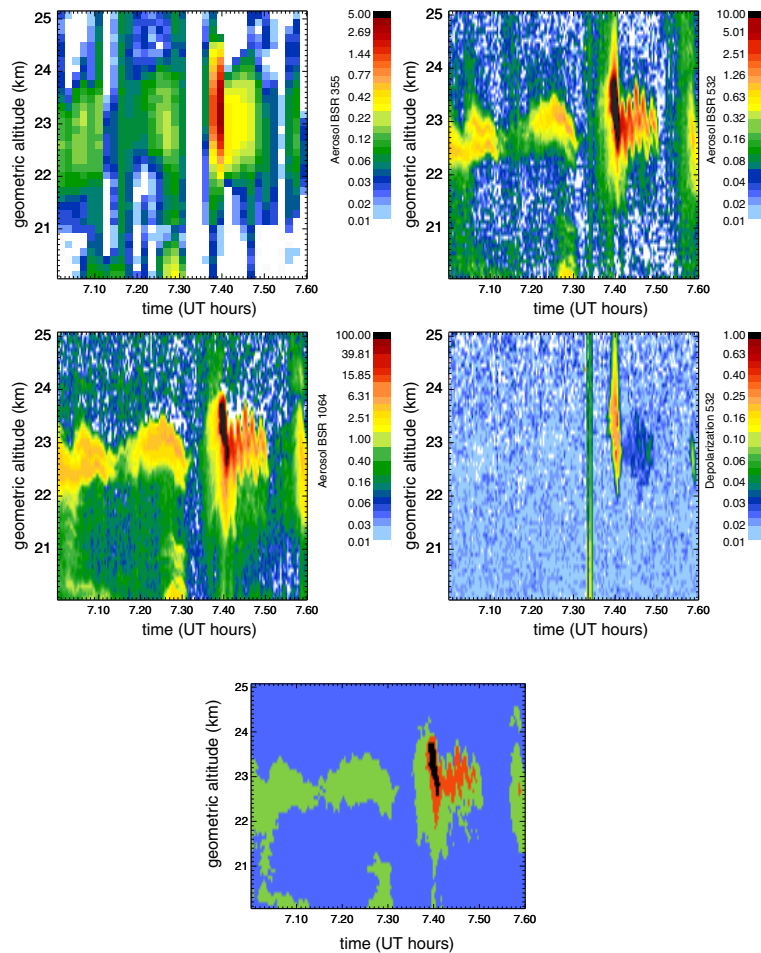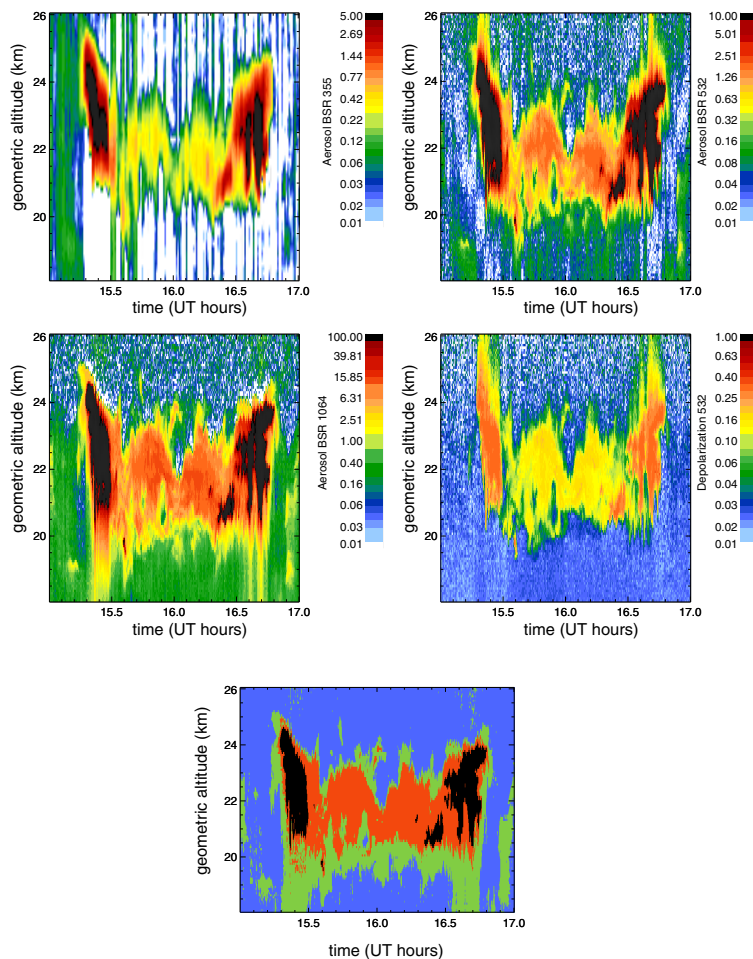
Plate 2. Lidar observations of polar stratospheric clouds during a flight on January 14, 2000. (a) backscatter ratio S at 354 nm laser wavelength; (b) backscatter ratio at 532 nm laser wavelength; (c) backscatter ratio at 1064 nm laser wavelength; (d) aerosol depolarization δ at 532 nm; (e) particle type assumed in the retrieval: background aerosol (blue), liquid PSC (green), NAT (red), ice (black).
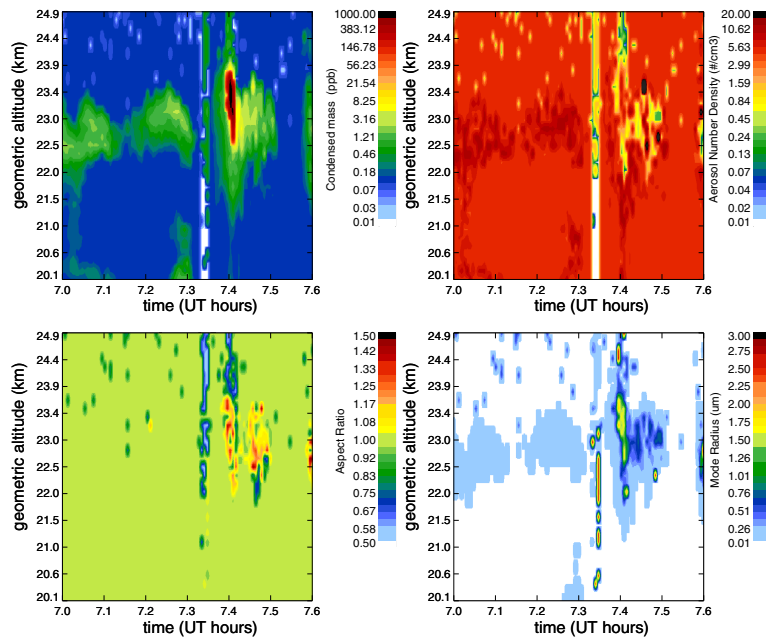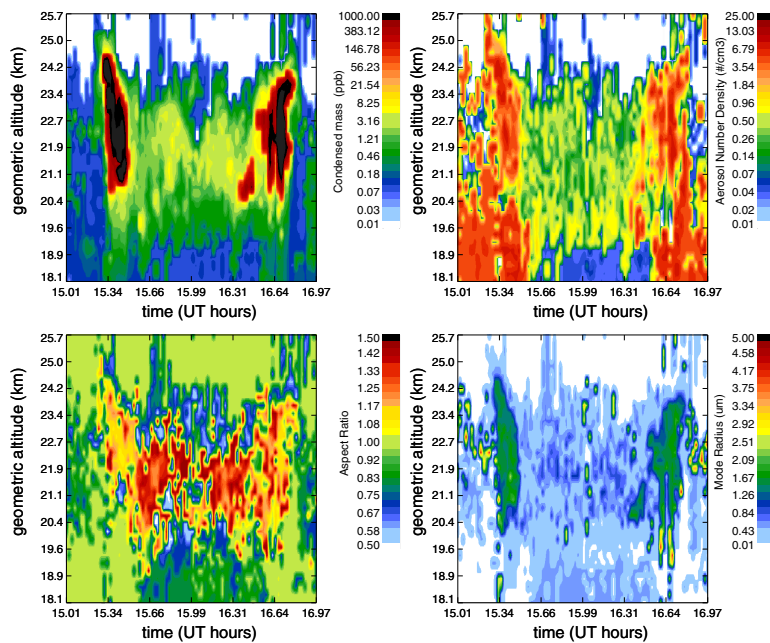
Plate 3. Retrieved aerosol properties from lidar measurements on January 14, 2000. (a) Condensed mass; (b) number density; (c) spheroidal aspect ratio; (d) mode radius. The speckled regions in (b), (c) and (d) indicate solution ambiguity. Non-speckled regions of the cloud indicate regions where the retrieved properties are most reliable.
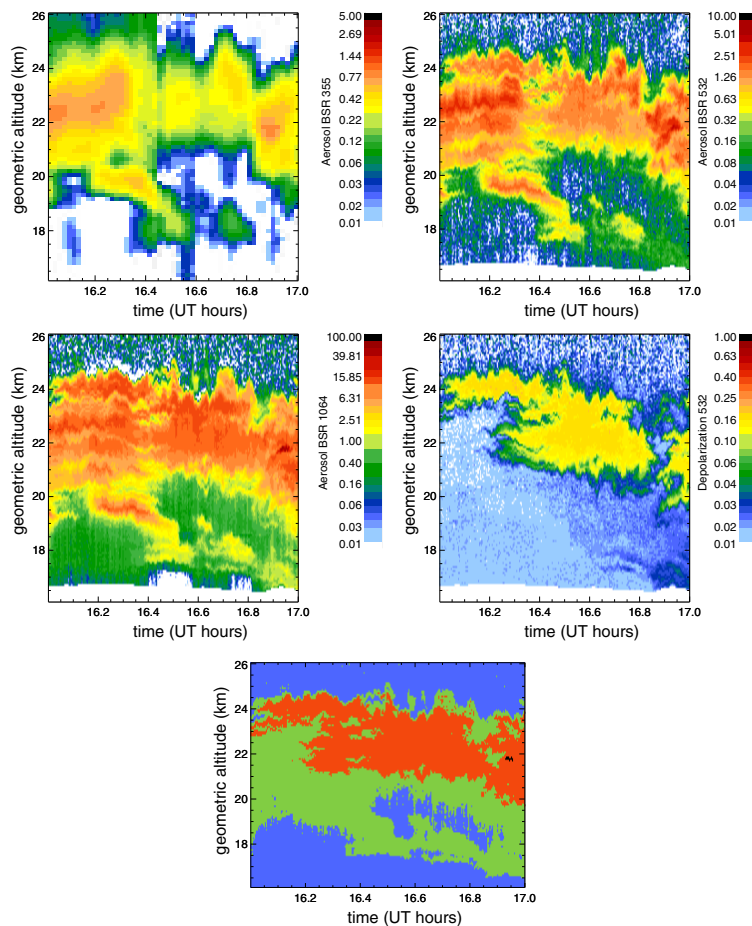
Plate 4. Lidar measurements of polar stratospheric clouds during a flight on January 25, 2000. (a) backscatter ratio S at 355 nm laser wavelength; (b) backscatter ratio at 532 nm laser wavelength; (c) backscatter ratio at 1064 nm laser wavelength; (d) aerosol depolarization δ at 532 nm; (e) particle type assumed in the retrieval: background aerosol (blue), liquid PSC (green), NAT (red), ice (black).
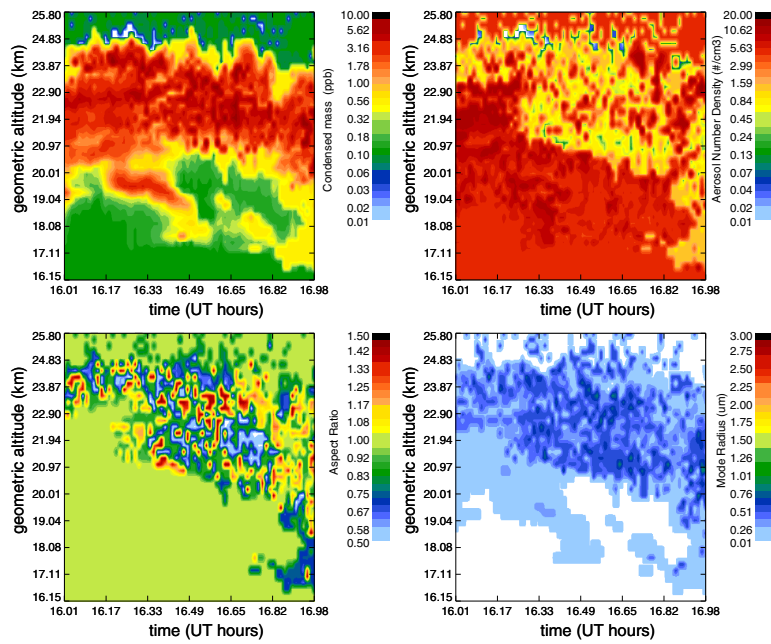
Plate 5. Retrieved aerosol properties from lidar measurements on January 25, 2000. (a) Condensed mass; (b) number density; (c) aspect ratio; (d) mode radius. The speckled regions in (b), (c) and (d) indicate solution ambiguity. Non-speckled regions of the cloud indicate regions where the retrieved properties are most reliable.

Plate 6. Lidar measurements of polar stratospheric clouds during a flight on January 23, 2000. (a) backscatter ratio S at 355 nm laser wavelength; (b) backscatter ratio at 532 nm laser wavelength; (c) backscatter ratio at 1064 nm laser wavelength; (d) aerosol depolarization δ at 532 nm; (e) particle type assumed in the retrieval: background aerosol (blue), liquid PSC (green), NAT (red), ice (black).

Plate 7. Retrieved aerosol properties from lidar measurements on January 23, 2000. (a) Condensed mass; (b) number density; (c) aspect ratio; (d) mode radius.
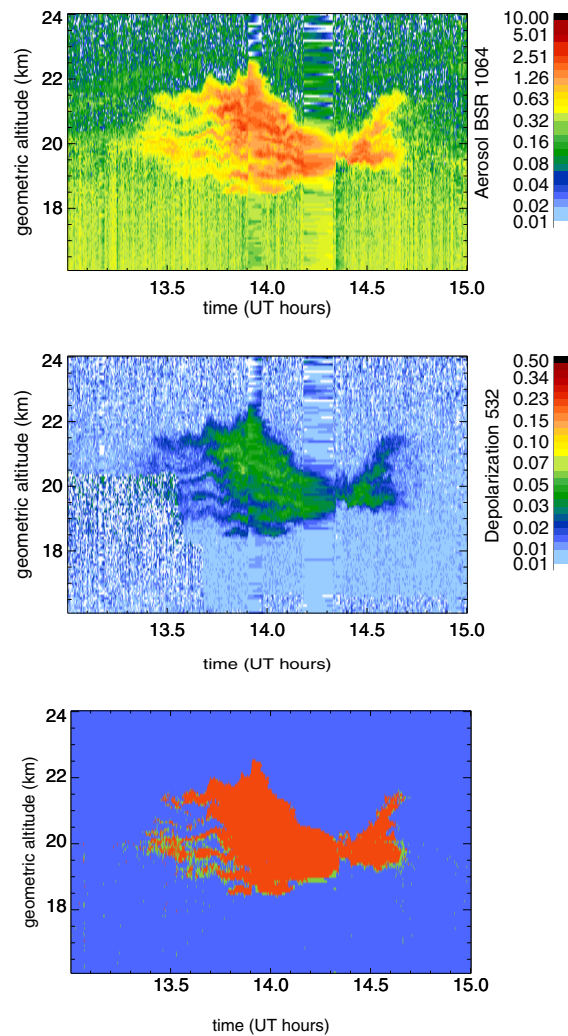
Plate 8. Lidar measurements of polar stratospheric clouds during a flight on December 10, 1999. (a) backscatter ratio S at 1064 nm laser wavelength; (b) aerosol depolarization δ at 532 nm; (c) particle type assumed in the retrieval: background aerosol (blue), liquid PSC (green), NAT (red), ice (black).
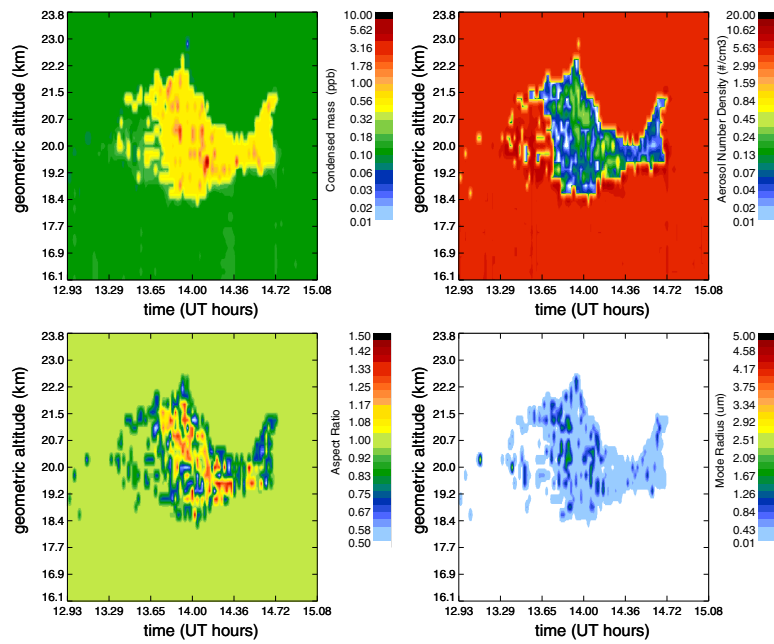
Plate 9. Retrieved aerosol properties from lidar measurements on December 10, 1999. (a) Condensed mass; (b) number density; (c) aspect ratio; (d) mode radius.